# **Evaluating noises of boson sampling with statistical benchmark methods**

Yang Ji<sup>1,2</sup>, Yongjin Ye<sup>2</sup>, Qiao Wang<sup>2</sup>, Shi Wang<sup>1,2</sup>, Jie Hou<sup>1,2</sup>, Yongzheng Wu<sup>\*1,2</sup>, Zijian Wang<sup>2</sup>, Bo Jiang<sup>\*2</sup>

<sup>1</sup>Shanghai Research Center for Quantum Sciences, Shanghai 201315, China

<sup>2</sup>The 32nd Research Institute of China Electronics Technology Group Corporation, Shanghai 201808, China

\*Corresponding authors. E-mails: 782613169@qq.com, b26jiang@126.com

### **Abstract**

The lack of self-correcting codes hiders the development of boson sampling to be large-scale and robust. Therefore, it is important to know the noise levels in order to cautiously demonstrate the quantum computational advantage or realize certain tasks. Based on those statistical benchmark methods such as the correlators and the clouds, which are initially proposed to discriminate boson sampling and other mockups, we quantificationally evaluate noises of photon partial distinguishability and photon loss compensated by dark counts. This is feasible owing to the fact that the output distribution unbalances are suppressed by noises, which are actually results of multi-photon interferences. This is why the evaluation performance is better when high order correlators or corresponding clouds are employed. Our results indicate that the statistical benchmark methods can also work in the task of evaluating noises of boson sampling.

**Keywords**: Boson sampling, statistical benchmark method, photon distinguishability, photon loss, dark count

The proposal of quantum computing systems is challenged by realistic noises, preventing them from working correctly in a large scale. As an essential light-based candidate among these systems, boson sampling has attracted great attentions because it is free from constructing quantum logic gates and thus practically simple [1, 2]. Until now, boson sampling has developed to demonstrate the so-called quantum computational advantages [3, 4], or realize certain tasks using its variants [5-10]. These are only guaranteed by the condition that the realistic noises are extremely low, otherwise the output deviations will entirely destroy the multi-photon interference trails and boson sampling will degenerate to be approximately classical [11-19], considering that self-correcting codes are absent. In these cases, the quantum advantage claims are unreliable even though the output photon number is large.

The main noises in the very original boson sampling are photon partial distinguishability [11, 16, 20] as well as photon loss [12, 16, 17, 21]. The former is due to the intrinsic photon differences such as those of locations and frequencies during the preparation of single-photon sources, while the latter is due to the imperfections of practical devices such as linear interferometers. Photon loss is easy to judge by just counting the output photon number, whereas it will be hided when it is compensated by dark counts happening in those detectors [22]. As a contrast, distinguishability is not intuitive. Both photon loss and distinguishability will suppress multi-photon interferences directly, resulting in the lack of quantum contributions in the overall probability distributions and making boson sampling easier to be classically simulated. For example, consider the classical simulation algorithm owing to Clifford and Clifford [23], of which the computation complexity is  $O[n2^n + ploy(m, n)]$ , where n and m are photon and mode numbers, it is easy to deduce that if the left photon number is scaled as  $O(\log_2 n)$ , then lossy boson sampling can be simulated by a classical computer in polynomial time [24]. As for distinguishability, the classical approximation algorithm using the cutoff interference photon number, owing to Renema [11], can simulate boson sampling within a little error of total variance distances, where only a finite interference scale is in need. Therefore, it is important to know noise levels, if one needs to estimate whether the results are from the quantum processes or not.

Of course, noises can be evaluated by calculating total variance distances of all the output patterns, which is computational inefficient [21]. Hence, it alternatively turns to those validation approaches [25-31] which initially only provide a binary judgement when dealing with boson sampling and other mockups, such as the mean-field sampling [32]. With this in mind, in our previous work [33], we extended the pattern recognition validation approach to evaluate noises of boson sampling, where both of the two main kind noises are considered. It is found that the extension is feasible based on the fact that the unbalanced distributions are suppressed by photon distinguishability, while the light-source happening photon loss will worsen the validation performances because of the introduced uncertainty of correspondent submatrices. The unbalance is essential based on the fact that it will responds to the main kind noises in a monotonous way. This motivates us to explore the extension of other validation schemes which may be easier to conduct, or may reveal the noise information in a much more determinate routine.

In this paper, we focus on the statistical benchmark methods such as the correlators and the correspondent clouds [31, 34], which are also computational efficient. In our opinions, there are at least two advantages with using these methods. Firstly, it is believed that those higher order correlators are naturally more sensitive to multi-photon interferences [33], which will vanish gradually with noises. Secondly, the statistical benchmark methods land on the framework where the random matrix theory works [31]. Therefore, one does not need to learn

the interferometer information, even though it is at the cost of much larger amounts of samples. This hints us that extracting the noise information from numerous output patterns may be relatively easy in boson sampling, or in some other quantum computing systems where finite noises are dominant.

In boson sampling, the probability of output pattern  $|T\rangle = |T_1, T_2, ..., T_m\rangle$  is determined by [1]

$$\Pr_{\text{ideal}}(T) = \frac{|\Pr(\mathbf{M}^{S,T})|^2}{\prod_{i=1}^m S_i! \prod_{i=1}^m T_i!},\tag{1}$$

where  $|S\rangle = |S_1, S_2, ..., S_m\rangle$  is the input Fock state and **M** is the interferometer matrix.  $\mathbf{M}^{S,T}$  is the submatrix by selecting the rows and columns of **M** according to the input and output states. Perm(·) denotes the matrix permanent, where the computation complexity is  $O(n2^n)$  using the best-known algorithm [24], if the complex matrix is Harr random. The output samples can be obtained with classical simulating algorithms such as the rejection [35], Markov Chain Monte Carlo [35], and the algorithm owing to Clifford and Clifford [23].

Here, three kinds of noises are taken into consideration, which are photon distinguishability, photon loss and dark counts. The latter two kind noises are discussed together because they can compensate with each other and make the output photon number equal to that of the input. Moreover, if one observes a pattern with fewer photons, one still can't exclude the case that some photons come from dark counts. Hence, it is hard to tell the noise levels by just counting the output photon numbers, no matter post selecting is used.

As for photon distinguishability, the pairwise noise information is collected by a tensor, in which case the output probability is [11]

$$\Pr_{\text{pd}}(T) = \frac{\sum_{\sigma} (\prod_{j=1}^{n} a_{\sigma_{j}j}) \Pr(\mathbf{M}^{S,T} \odot \mathbf{M}_{1,\sigma}^{S,T*})}{\prod_{i=1}^{m} S_{i}! \prod_{i=1}^{m} T_{i}!}.$$
 (2)

 $\sigma = \{\sigma_1, ..., \sigma_n\}$  runs over all the permutations of  $\{1, ..., n\}$  and  $a_{ij} = x_{\text{ind}} + (1 - x_{\text{ind}})\delta_{ij}$  is the tensor element. We can use the value  $x_{\text{ind}}$  as the signature of distinguishability. When  $x_{\text{ind}} = 1$  photons are indistinguishable and when  $x_{\text{ind}} = 0$  photons are totally distinguishable.  $\mathbf{M}_{1,\sigma}^{S,T}$  is a rearrangement of  $\mathbf{M}^{S,T}$ , where the columns are rearranged according to  $\sigma$ .  $\odot$  is the elementwise product.

It is possible to employ those well-known classical algorithms to exactly simulate boson sampling with photon distinguishability. Here, we employ the Clifford-Clifford algorithm, which is usually used for ideal boson sampling [23], by noticing that  $1 - x_{\text{ind}}$  actually is equivalent to the probability of a photon becoming totally distinguishable compared to others and entering into a virtual mode through a virtual beam splitter, which is similar to the Gaussian boson sampling cases [18], as shown in Fig .1. For the *i*th input photon (i = 1,...,n), the

extended m(n+1)-dimensional matrix  $\mathbf{B}_i$  of the virtual beam splitter between the *i*th (actual) mode and the i(m+1)-th (virtual) mode, is a revision of the identity matrix, where the revised 4 elements become  $b_{i,i} = \cos \omega$ ,  $b_{i,i(m+1)} = -\sin \omega$ ,  $b_{i(m+1),i} = \sin \omega$ ,  $b_{i(m+1),i(m+1)} = \cos \omega$ .  $\cos \omega$  is the reflectivity of the beam splitter, which is related with  $x_{ind}$  via

$$\cos^2 \omega = x_{\text{ind}}.$$
 (3)

For n partially distinguishable photons, n individual virtual m-mode interferometers characterized by  $\mathbf{M}$  are constructed in Fig. 1, along with n virtual beam splitters  $\mathbf{B}_1,...,\mathbf{B}_n$ . Therefore, the overall optical network matrix, including those actual and virtual parts, can be written as

$$\mathbf{U} = \mathbf{B}_1 \dots \mathbf{B}_n(\bigoplus_{i=1}^{n+1} \mathbf{M}). \tag{4}$$

Indeed, **U** has already contained the noise information of photon distinguishability. Correspondingly, the input state is now  $|S'\rangle = |S_1, S_2, ..., S_m, 0, ..., 0\rangle$ , with zero states as the input for those virtual modes. Based on these, the Clifford-Clifford algorithm can now be employed, where the remaining work is to collect those photons measured in the actual and virtual detectors at the mode terminals, labelled by the same number in Fig.1, into one actual detector for one measurement time. The introduction of virtual optical parts will not greatly increase the computational complexity of the algorithm because it is only polynomial to the mode number. Equivalently, the simulations can also be carried out with the Clifford-Clifford algorithm, by using the scheme that for each input photon, it will be sent into the virtual interferometer characterized by **M** alone, with the probability of  $1 - x_{ind}$ , where the simulation algorithm is then performed.

As for photon loss, we use the balanced loss model, where for each mode, the photon transmittance is assumed to be constant [17]. This is suitable for a common symmetric interferometer with the optical unit number and the depth scaled as  $O(m^2)$  and O(m) respectively [36]. In this model, for each output photon, the loss probability is kept the same. Hence, the output photon number in each mode follows a binomial distribution and thus we can write down the output probability as

$$Pr_{loss}(T) = \sum_{T'} \{ pr_{ideal}(T') \prod_{i=1}^{m} [\binom{T'_i}{T_i} \eta_t^{T_i} (1 - \eta_t)^{T'_i - T_i} ] \},$$
 (5)

where T' runs over all the *n*-photon output patterns with  $T'_i \ge T_i$ ,  $\forall i$ , and *n* is now the input photon number.  $\eta_t$  is the transmission rate of each mode. Higher  $\eta_t$  corresponds to a lower photon loss probability.

Dark counts are only dependent on photon detector qualities and usually the correspondent dark counting probability is quite low [22]. It is only necessary to consider this noisy effect when m is extremely large. For example, in the collision-free regime where  $m = O(n^2)$  [24],

if the dark counting probability  $p_{\rm dc}$  is constant and the redundant photon number is scaled as o(m), then it will be comparative to the effective photon number n when m is extremely large. Despite in general, dark counts are expected to have little influences on realizing the quantum computational advantage due to quite low  $p_{\rm dc}$ , it will worsen those large-scale implement performances more or less. Note that with photon loss and dark counts, the photon number fluctuations will not improve the computation complexity because the two kind noises have no influences to the background probabilities. Based on the fact that the dark counting probability is constant for each detector, and thus, the dark counting detector number follows a binominal distribution, we can obtain the output probability via

$$Pr_{dc}(T) = \sum_{T'} [pr_{ideal}(T')(1 - p_{dc})^{m+n-\sum_{i}T_{i}} p_{dc} \sum_{i} T_{i} - n], \tag{6}$$

where T' now runs over all the n-photon output patterns with  $0 \le T_i - T_i' \le 1$ ,  $\forall i$ . Writing down the output probabilities considering both photon loss and dark counts is relatively complex because of numerous combinations. However, as for simulations, one only needs to change the original output patterns obtained based on Eq. (1), according to the binominal distributions mentioned above. Here the Clifford-Clifford algorithm is also used to simulate those original ideal samples. We are interested in those patterns with n photons because other patterns can be excluded by post selecting.

We extend the statistical benchmark validation methods to evaluate noises, by observing the mean photon number products of different mode combinations. More specifically, the *t*th-order correlator is expressed as [34]

$$\kappa(n_{o_1}, ..., n_{o_t}) = \sum_{\pi} [(|\pi| - 1)! (-1)^{|\pi| - 1} \prod_{B \in \pi} \langle \prod_{i \in B} n_{o_i} \rangle]. \tag{7}$$

 $\{o_1, ..., o_t\} \subseteq \{1, ..., m\}$  is the selected output mode number list without repetitions.  $n_{o_i}$  is the photon number in  $o_i$ -th mode.  $\pi$  runs over all the partitions of  $\{1, ..., t\}$ . By observing Eq. (7), we know the 1st-order correlator is  $\langle n_i \rangle$ ,  $i \in \{1, ..., m\}$ . This reveals little noise information because  $\sum_i \langle n_i \rangle = n$  is fixed and there are only m correlators, which is much fewer compared to those higher order correlators. More importantly, multi-photon interferences are more sensitive to noises [33], which are mainly revealed by higher order correlators. Fig. 2 shows the 2nd to 4th order correlators with changing photon partial distinguishability. It is visualized to find that with increasing  $x_{\text{ind}}$ , those correlator points become closer to the line x = y. That is to say, the correspondent correlators become similar to the ideal ones gradually with increasing  $x_{\text{ind}}$ .

We first extract noise information by calculating Pearson and Spearman correlation coefficients according to Fig. 2. It is found that with increasing  $x_{ind}$ , both the correlation coefficients grow in tendency, which are more obvious with higher order correlators, as shown in Fig. 3. However, some points may drop slightly with  $x_{ind}$  even for those higher order correlators. This indicates that the correlation coefficients can only provide coarse evaluations of noises.

We alternatively investigate the point deviations in Fig. 2 by calculating  $\gamma = (\sum_i \kappa_{\text{test},i})/(\sum_i \kappa_{\text{comp},i})$ , where  $\kappa_{\text{test},i}$  and  $\kappa_{\text{comp},i}$  are *i*th test and compared correlators. The correspondent tendencies are presented in Fig. 3 (c), where the changes are obviously more continuous. The changes become sharp when the photons are close to be indistinguishable. This is because only when  $\kappa_{\text{ind}}$  is relatively high, the multi-photon interferences become significant, otherwise the processes tend to be classical. Indeed, the higher order correlators provide better evaluation performances, whereas it is at the cost of computation time because for the *t*-order, there are  $\binom{m}{t}$  correlators in total to consider. The evaluations are affected by boson sampling scales. As shown in Fig. 4, with increasing *n* or decreasing *m*, the deviations become obvious for those samples with distinguishability when compared to the ideal ones. Note that with increasing *m*,  $\gamma$  with  $\kappa_{\text{ind}} = 0$  only grows asymptotically in the inset of Fig. 4 (b), indicating that the correlation method is robust even when *m* is large.

We furtherly extend the cloud method [31] by observing the coefficient of variation (CV) and the coefficient of skewness (CS), based on the correlators. This is believed to be free from learning the interferometer matrix information which usually is at the cost of extra experiments [37]. We alternatively make our results close to the expectation values according to the random matrix theory, through going over all the possible single-photon input combinations, in the regime  $m \gg n$ . Fig. 5 presents the clouds formed based on the 2nd and 3rd order correlators. The clouds shift gradually with changing  $x_{\rm ind}$ . This is more obvious for 3rd order correlators, indicating once again that the higher order correlators indeed have a better evaluation performance. The mean CV and CS values of the clouds are shown in Fig. 5, where values based on higher order correlators change more greatly. It is found that the mean CV is sensitive to higher  $x_{\rm ind}$  while the mean CS is more sensitive to moderate  $x_{\rm ind}$ . In a word, we can evaluate the noise of photon partial distinguishability based on the cloud method, without learning interferometer information.

Next, we focus on the extended statistical benchmark methods on evaluating the noises of photon loss compensated by dark counts, with n-photon output patterns. For simplicity, we keep the condition that  $1 - \eta_t = p_{loss} = p_{dc} = p_{noise}$ . Note that in general,  $p_{dc}$  is quite low and the condition is not realistic. We just use this extreme condition to test the performances of statistical benchmark methods. The noise evaluations are presented in Fig. 6. With enhancing the noise level,  $\gamma$  decreases in tendency, whereas some points may be deviated from the tendency especially when the noise level is quite low. As for the cloud method, the changes of mean CS and CV are continuous with the noise level.

Note that in Fig. 6, when the noise level is quite low, the evaluations go through poor performances with drastic fluctuations or inapparent changes, which is totally contrast to the photon partial distinguishability case. We furtherly investigate the influences of  $p_{\text{noise}}$  by

observing the distributions of sorted output patterns. The probability calculations of all the output patterns are relatively difficult because of numerous combinations when  $p_{\text{noise}}$  is not zero. However, we can obtain the distributions approximately by simulating massive amounts of samples since the simulations are simple with fixed background probabilities. The distributions in Fig. 7 (a) indicate that only when  $p_{\text{noise}}$  is relatively high, the probability deviations are obvious, leading to the vanishment of unbalances. Indeed, it can be understood by considering the process that the unbalanced distribution is first partly eliminated by photon loss, and then replaced by a more balanced one due to dark counts.

The deviations can also be evaluated by the total variance distance  $D = \frac{1}{2} \sum_{T} |\Pr_{\text{noise}}(T) - \Pr_{\text{ideal}}(T)|$  [21], where  $\Pr_{\text{noise}}(T)$  and  $\Pr_{\text{ideal}}(T)$  are probabilities of the output pattern T with and without noises. As shown in Fig. 7 (b), the enhancement of D is first suppressed when the noise level is quite low, in which region the statistical benchmark methods have poor performances. As a contrast, as for the noise of photon partial distinguishability, when  $x_{\text{ind}}$  is slightly deviated from 1, the enhancement of D is obvious.

In conclusion, we have observed the success of quantificationally evaluating noises in boson sampling using statistical benchmark methods, which are computational efficient. These methods are found to be more effective when higher order correlators are used, which are more sensitive to multi-photon interferences. The cloud method performs well, working in the regime  $m\gg n$  and free from learning interferometer information. We notice that the noises of photon loss compensated by dark counts can also lead to the vanishment of output distribution unbalances. Our results provide a routine to evaluate noises in certain quantum computing systems, where some dominant noises may influence the output data structure gradually, with the assistant of statistical benchmark methods.

Acknowledgements. This work can be carried out thanks to Project supported by Shanghai Municipal Science and Technology Major Project (Grant No. 2019SHZDZX01), and three projects supported by the 32nd Research Institute of China Electronics Technology Group Corporation (Grant No. DC240554-00, Grant No. AG231031-00 and Grant No. AG230639-00).

## References

[1] Aaronson, S.; Arkhipov, A. The computational complexity of linear optics. In Proceedings of the forty-third annual ACM symposium on Theory of computing, San Jose, California, USA; 2011.

[2] Hamilton, C. S.; Kruse, R.; Sansoni, L.; Barkhofen, S.; Silberhorn, C.; Jex, I. Gaussian Boson Sampling. *Physical Review Letters* **2017**, *119* (17), 170501. DOI: 10.1103/PhysRevLett.119.170501.

- [3] Deng, Y.-H.; Gu, Y.-C.; Liu, H.-L.; Gong, S.-Q.; Su, H.; Zhang, Z.-J.; Tang, H.-Y.; Jia, M.-H.; Xu, J.-M.; Chen, M.-C.; et al. Gaussian Boson Sampling with Pseudo-Photon-Number-Resolving Detectors and Quantum Computational Advantage. *Physical Review Letters* **2023**, *131* (15), 150601. DOI: 10.1103/PhysRevLett.131.150601.
- [4] Deshpande, A.; Mehta, A.; Vincent, T.; Quesada, N.; Hinsche, M.; Ioannou, M.; Madsen, L.; Lavoie, J.; Qi, H.; Eisert, J.; et al. Quantum computational advantage via high-dimensional Gaussian boson sampling. *Science Advances* **2022**, *8* (1), eabi7894. DOI: doi:10.1126/sciadv.abi7894.
- [5] Shi, J.; Zhao, T.; Wang, Y.; Yu, C.; Lu, Y.; Wu, J.; Shi, R.; Zhang, S.; Peng, S.; Wu, J. An Unbiased Quantum Random Number Generator Based on Boson Sampling. *Advanced Quantum Technologies* **2024**, *7* (1), 2300179. DOI: https://doi.org/10.1002/qute.202300179.
- [6] Huh, J.; Guerreschi, G. G.; Peropadre, B.; McClean, J. R.; Aspuru-Guzik, A. Boson sampling for molecular vibronic spectra. *Nature Photonics* **2015**, *9* (9), 615-620. DOI: 10.1038/nphoton.2015.153.
- [7] Banchi, L.; Fingerhuth, M.; Babej, T.; Ing, C.; Arrazola, J. M. Molecular docking with Gaussian Boson Sampling. *Science Advances* **2020**, *6* (23), eaax1950. DOI: doi:10.1126/sciadv.aax1950.
- [8] Deng, Y.-H.; Gong, S.-Q.; Gu, Y.-C.; Zhang, Z.-J.; Liu, H.-L.; Su, H.; Tang, H.-Y.; Xu, J.-M.; Jia, M.-H.; Chen, M.-C.; et al. Solving Graph Problems Using Gaussian Boson Sampling. *Physical Review Letters* **2023**, *130* (19), 190601. DOI: 10.1103/PhysRevLett.130.190601.
- [9] Arrazola, J. M.; Bromley, T. R. Using Gaussian Boson Sampling to Find Dense Subgraphs. *Physical Review Letters* **2018**, *121* (3), 030503. DOI: 10.1103/PhysRevLett.121.030503.
- [10] Brádler, K.; Dallaire-Demers, P.-L.; Rebentrost, P.; Su, D.; Weedbrook, C. Gaussian boson sampling for perfect matchings of arbitrary graphs. *Physical Review A* **2018**, *98* (3), 032310. DOI: 10.1103/PhysRevA.98.032310.
- [11] Renema, J. J.; Menssen, A.; Clements, W. R.; Triginer, G.; Kolthammer, W. S.; Walmsley, I. A. Efficient Classical Algorithm for Boson Sampling with Partially Distinguishable Photons. *Physical Review Letters* **2018**, *120* (22), 220502. DOI: 10.1103/PhysRevLett.120.220502.
- [12] Renema J.; Shchesnovich V.; Garcia-Patron R. Classical Simulability of Noisy Boson Sampling. arXiv:1809.01953. DOI: https://doi.org/10.48550/arXiv.1809.01953.
- [13] Oh, C.; Noh, K.; Fefferman, B.; Jiang, L. Classical simulation of lossy boson sampling using matrix product operators. *Physical Review A* **2021**, *104* (2), 022407. DOI: 10.1103/PhysRevA.104.022407.

- [14] Liu, M.; Oh, C.; Liu, J.; Jiang, L.; Alexeev, Y. Simulating lossy Gaussian boson sampling with matrix-product operators. *Physical Review A* **2023**, *108* (5), 052604. DOI: 10.1103/PhysRevA.108.052604.
- [15] Oh, C.; Liu, M.; Alexeev, Y.; Fefferman, B.; Jiang, L. Classical algorithm for simulating experimental Gaussian boson sampling. *Nature Physics* **2024**, *20* (9), 1461-1468. DOI: 10.1038/s41567-024-02535-8.
- [16] Moylett, A. E.; García-Patrón, R.; Renema, J. J.; Turner, P. S. Classically simulating near-term partially-distinguishable and lossy boson sampling. *Quantum Science and Technology* **2020**, *5* (1), 015001. DOI: 10.1088/2058-9565/ab5555.
- [17] Oszmaniec, M.; Brod, D. J. Classical simulation of photonic linear optics with lost particles. *New Journal of Physics* **2018**, *20* (9), 092002. DOI: 10.1088/1367-2630/aadfa8.
- [18] Shi, J.; Byrnes, T. Effect of partial distinguishability on quantum supremacy in Gaussian Boson sampling. *npj Quantum Information* **2022**, *8* (1), 54. DOI: 10.1038/s41534-022-00557-9.
- [19] Shchesnovich, V. S. Noise in boson sampling and the threshold of efficient classical simulatability. *Physical Review A* **2019**, *100* (1), 012340. DOI: 10.1103/PhysRevA.100.012340.
- [20] Tichy, M. C. Sampling of partially distinguishable bosons and the relation to the multidimensional permanent. *Physical Review A* **2015**, *91* (2), 022316. DOI: 10.1103/PhysRevA.91.022316.
- [21] Wang, H.; Li, W.; Jiang, X.; He, Y. M.; Li, Y. H.; Ding, X.; Chen, M. C.; Qin, J.; Peng, C. Z.; Schneider, C.; et al. Toward Scalable Boson Sampling with Photon Loss. *Physical Review Letters* **2018**, *120* (23), 230502. DOI: 10.1103/PhysRevLett.120.230502.
- [22] Arrazola, J. M.; Diamanti, E.; Kerenidis, I. Quantum superiority for verifying NP-complete problems with linear optics. *npj Quantum Information* **2018**, *4* (1), 56. DOI: 10.1038/s41534-018-0103-1.
- [23] Clifford, P.; Clifford, R. The Classical Complexity of Boson Sampling. In *Proceedings of the 2018 Annual ACM-SIAM Symposium on Discrete Algorithms (SODA)*, pp 146-155.
- [24] Daniel, J. B.; Ernesto, F. G.; Andrea, C.; Roberto, O.; Nicolò, S.; Fabio, S. Photonic implementation of boson sampling: a review. *Advanced Photonics* **2019**, *1* (3), 034001. DOI: 10.1117/1.AP.1.3.034001.
- [25] Bentivegna, M.; Spagnolo, N.; Vitelli, C.; Brod, D. J.; Crespi, A.; Flamini, F.; Ramponi, R.; Mataloni, P.; Osellame, R.; Galvão, E. F.; et al. Bayesian approach to Boson sampling validation. *International Journal of Quantum Information* **2014**, *12* (07n08), 1560028. DOI:

- 10.1142/s021974991560028x.
- [26] Dai, Z.; Liu, Y.; Xu, P.; Xu, W.; Yang, X.; Wu, J. A Bayesian validation approach to practical boson sampling. *Science China Physics, Mechanics & Astronomy* **2020**, *63* (5), 250311. DOI: 10.1007/s11433-019-1440-y.
- [27] Agresti, I.; Viggianiello, N.; Flamini, F.; Spagnolo, N.; Crespi, A.; Osellame, R.; Wiebe, N.; Sciarrino, F. Pattern Recognition Techniques for Boson Sampling Validation. *Physical Review X* **2019**, *9* (1), 011013. DOI: 10.1103/PhysRevX.9.011013.
- [28] Anguita M. C.; Camillini A.; Marzban S.; Robbio M.; Seron B.; Novo L.; Renema J. J. Experimental Validation of Boson Sampling Using Detector Binning. arXiv:2502.05093. DOI: https://doi.org/10.48550/arXiv.2502.05093.
- [29] Bressanini G.; Seron B.; Novo L.; Cerf N. J.; Kim M. S. Gaussian Boson Sampling Validation via Detector Binning. arXiv:2310.18113. DOI: https://doi.org/10.48550/arXiv.2310.18113.
- [30] Giordani, T.; Mannucci, V.; Spagnolo, N.; Fumero, M.; Rampini, A.; Rodolà, E.; Sciarrino, F. Certification of Gaussian Boson Sampling via graphs feature vectors and kernels. *Quantum Science and Technology* **2023**, *8* (1), 015005. DOI: 10.1088/2058-9565/ac969b.
- [31] Walschaers, M.; Kuipers, J.; Urbina, J.-D.; Mayer, K.; Tichy, M. C.; Richter, K.; Buchleitner, A. Statistical benchmark for BosonSampling. *New Journal of Physics* **2016**, *18* (3), 032001. DOI: 10.1088/1367-2630/18/3/032001.
- [32] Tichy, M. C.; Mayer, K.; Buchleitner, A.; Mølmer, K. Stringent and Efficient Assessment of Boson-Sampling Devices. *Physical Review Letters* **2014**, *113* (2), 020502. DOI: 10.1103/PhysRevLett.113.020502.
- [33] Ji, Y.; Wu, Y.; Wang, S.; Hou, J.; Chen, M.; Ni, M. Extension of a pattern recognition validation approach for noisy boson sampling. *Quantum Information Processing* **2025**, *24* (3), 91. DOI: 10.1007/s11128-025-04705-w.
- [34] Martínez-Cifuentes J.; Fonseca-Romero K. M.; Quesada N. Classical models may be a better explanation of the Jiuzhang 1.0 Gaussian Boson Sampler than its targeted squeezed light model. *Quantum* **2023**, *7*, 1076. DOI: https://doi.org/10.22331/q-2023-08-08-1076.
- [35] Neville, A.; Sparrow, C.; Clifford, R.; Johnston, E.; Birchall, P. M.; Montanaro, A.; Laing, A. Classical boson sampling algorithms with superior performance to near-term experiments. *Nature Physics* **2017**, *13* (12), 1153-1157. DOI: 10.1038/nphys4270.
- [36] Clements, W. R.; Humphreys, P. C.; Metcalf, B. J.; Kolthammer, W. S.; Walmsley, I. A. Optimal design for universal multiport interferometers. *Optica* **2016**, *3* (12), 1460-1465. DOI:

#### 10.1364/OPTICA.3.001460.

[37] Spring, J. B.; Metcalf, B. J.; Humphreys, P. C.; Kolthammer, W. S.; Jin, X.-M.; Barbieri, M.; Datta, A.; Thomas-Peter, N.; Langford, N. K.; Kundys, D.; et al. Boson Sampling on a Photonic Chip. *Science* **2013**, *339* (6121), 798-801. DOI: doi:10.1126/science.1231692.

# **Figures**

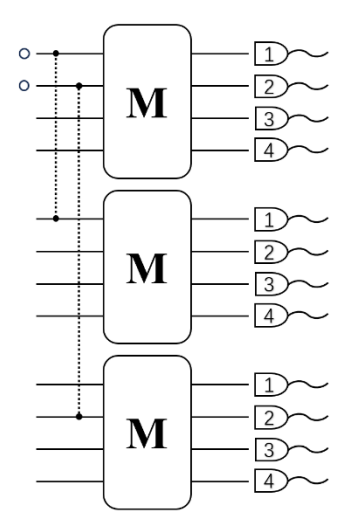


Fig. 1 Equivalent optical network of boson sampling with the noise of photon distinguishability. In this sketch, n=2 partially distinguishable photons enter into the interferometer characterized by  $\mathbf{M}$  with m=4. The first interferometer is actual while the last two are virtual. The dot lines represent the virtual beam splitters between actual and virtual modes.

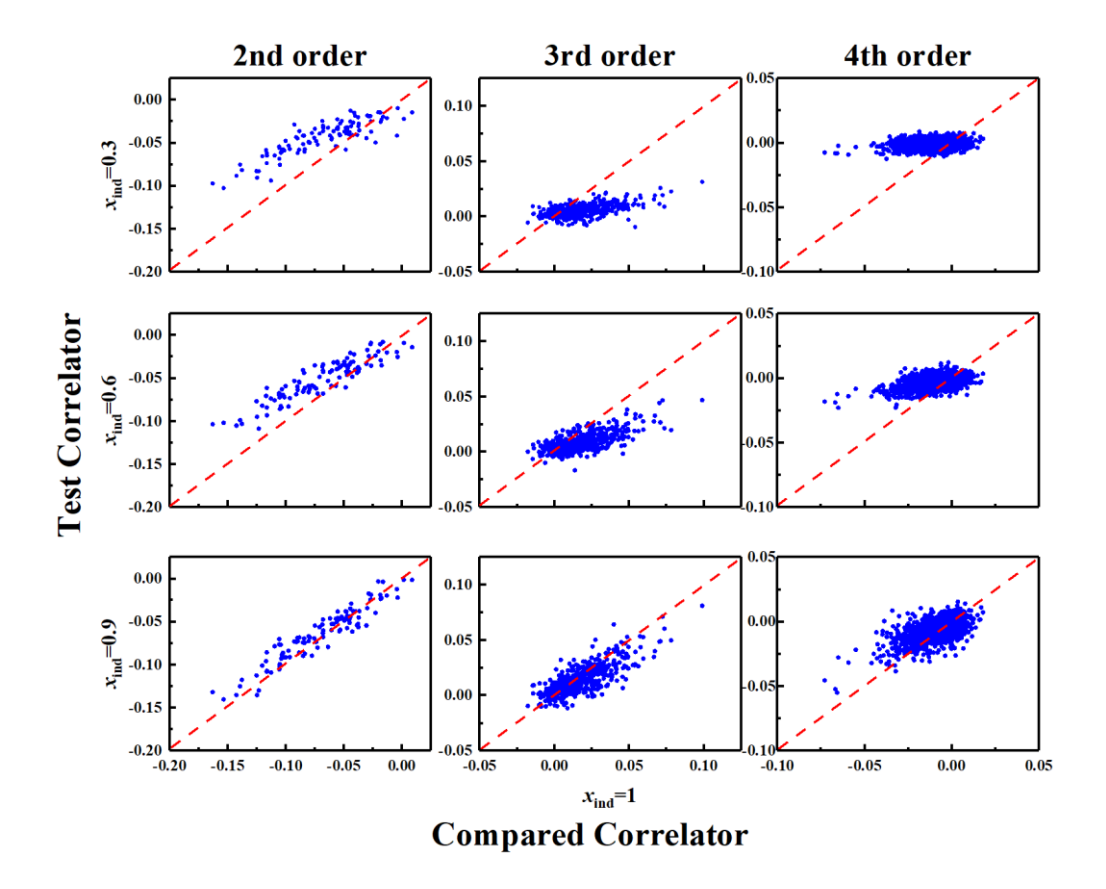


Fig. 2 Correlators for boson sampling with the noise of photon partial distinguishability. For each  $x_{\text{ind}}$ ,  $10^4$  samples are generated by simulation algorithms to obtain the correlators with n = 10 and m = 15. The red dash line is x = y.

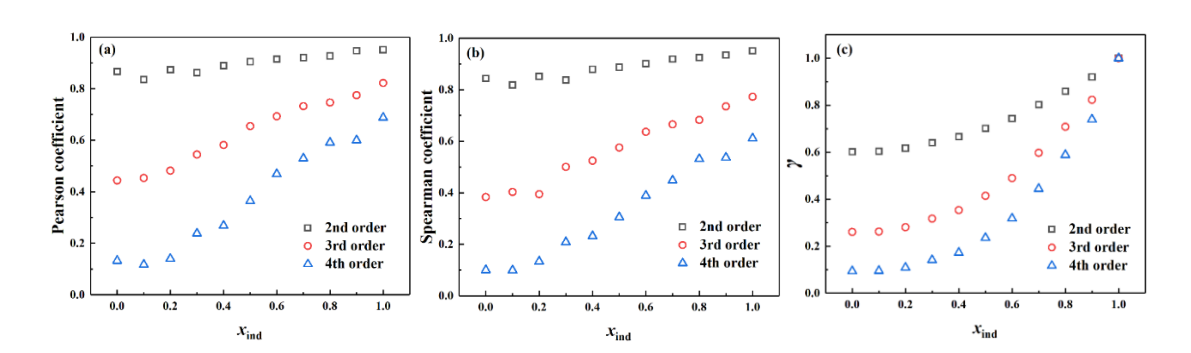


Fig. 3 Plots of relative coefficients and  $x_{ind}$ . (a) Pearson coefficients. (b) Spearman coefficients. (c)  $\gamma$  reflecting the point deviations.

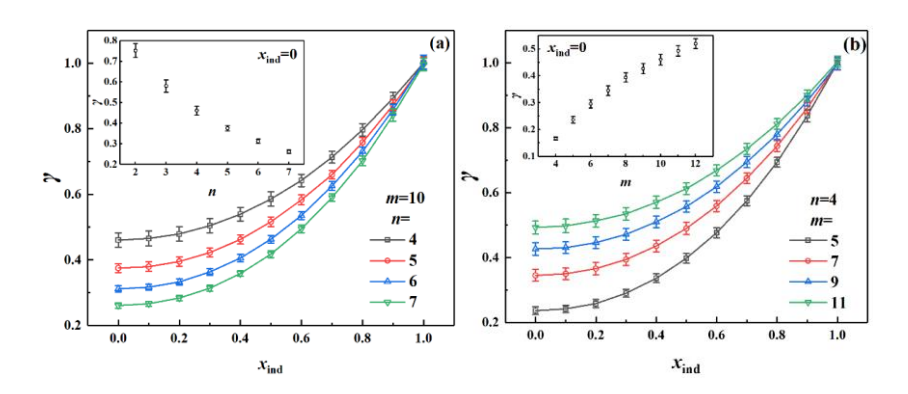


Fig. 4 Plots of  $\gamma$  and  $x_{\text{ind}}$  with different scales, where the correlation order t is 3. (a) m is fixed and n is changed. (b) n is fixed and m is changed. For each  $x_{\text{ind}}$ , 100 random matrices are generated as the interferometer matrices. For each matrix,  $10^4$  samples are generated to test. The insets show  $\gamma$  values changed with scales where  $x_{\text{ind}} = 0$ . The bars present the standard deviations.

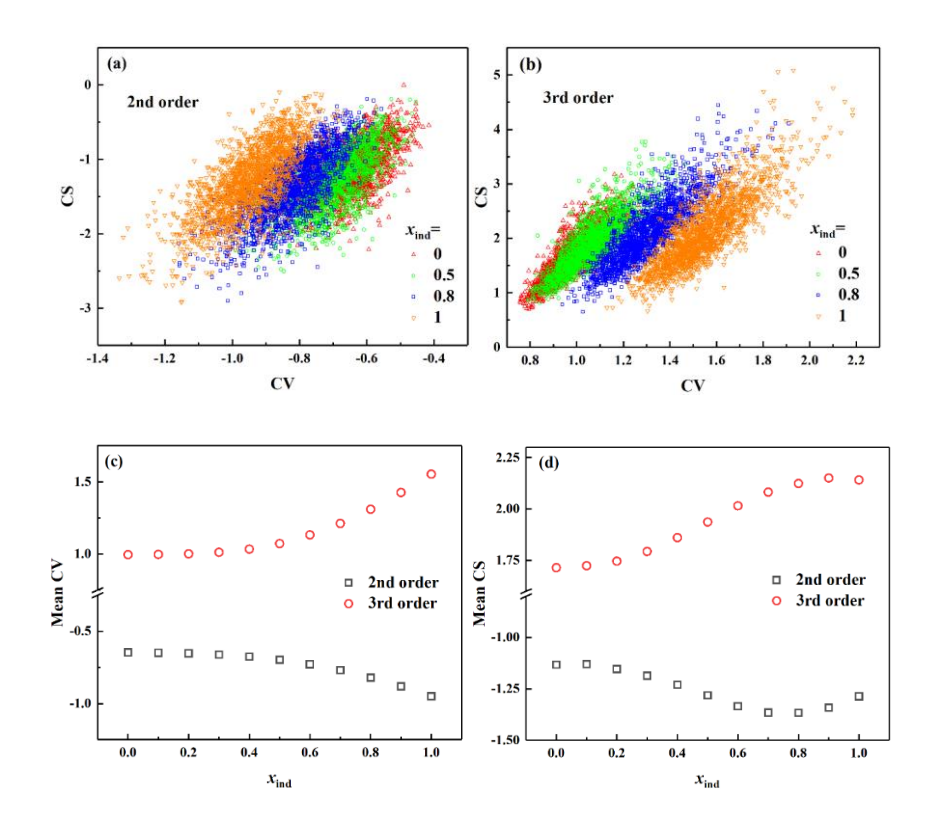


Fig. 5 The cloud method to evaluate the noise of photon partial distinguishability. (a)-(b) The clouds based on 2nd and 3rd order correlators, with n=4 and m=16. The sample number for each input combination and  $x_{\rm ind}$  is  $10^4$ . (c)-(d) Mean CV and CS values obtained based on the clouds with  $x_{\rm ind}$ .

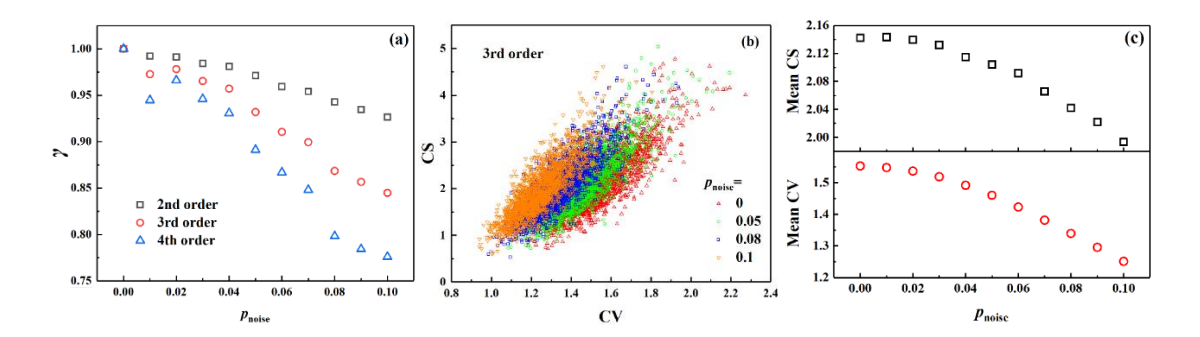


Fig. 6 The extended statistical benchmark methods for boson sampling with photon loss compensated by dark counts. (a) Plots of  $\gamma$  and  $p_{\text{noise}}$  based on the 2nd to 4th order correlators, where n=10, m=15 and the individual sample number is  $2\times10^4$ . (b) The clouds based on the 3rd order correlators with changing single-photon input combinations, where n=4, m=16 and the individual sample number is  $10^4$ . (c) Plots of mean CS (CV) and  $p_{\text{noise}}$  according to (b).

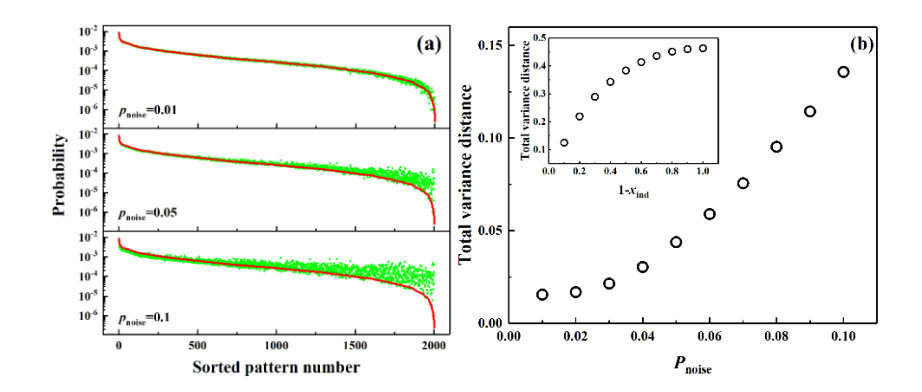


Fig. 7 Output probability deviations with noises. (a) Distributions of sorted output patterns with  $p_{\rm noise}$ . The red lines show the background distributions with n=5 and m=10, where the patterns are sorted according to the probabilities from high to low. The green dots present distributions of the correspondent patterns changed with  $p_{\rm noise}$ , which are obtained approximately by simulating  $10^6$  samples for each  $p_{\rm noise}$ . (b) Plots of the correspondent total variance distance and  $p_{\rm noise}$ . The inset shows plots with changing  $x_{\rm ind}$ .